Trans. JSASS Aerospace Tech. Japan
Vol. 14, No. ists31, pp.Pd_1 - Pd_8, 2017

ISTS-2017-d-059／ISSFD-2017-059

Nonlinear Uncertainty Propagation of Orbital Mechanics Subject to Stochastic Error in Atmospheric Mass Density Models

By Changyong HE,[1),2)] Yang YANG,[1),2)] Brett CARTER[2)] Han CAI[1),2)] Suqin WU[2)] and Kefei ZHANG[2)]

[1)] *Space Environment Research Centre (SERC) Limited, Australia*
[2)] *Satellite Positioning for Atmosphere, Climate and Environment (SPACE) Research Centre, School of Sciences, RMIT University, Australia*

(Received April 17th, 2017)

Without consideration of stochastic forces, orbital dynamical systems are expressed by ordinary differential equations (ODE) and its orbital uncertainty propagation (OUP) can be solved by one of the following methods: Monte Carlo simulations (MCS), state transition tensors, polynomial chaos expansion, etc. While the stochastic forces or diffusion (e.g., the stochastic force from the error in atmospheric mass density (AMD) models) may exert a large effect on a long-term OUP of nonlinear dynamical systems. The OUP expressed by stochastic differential equations (SDE) remains an unsolved problem due to its high dimensionality and nonlinearity.

Currently, the Fokker-Planck equation (FPE), a powerful tool for OUP, has been used to propagate the probability density function (PDF) of the orbital state. However, numerical methods used to solve the FPE suffer from the curse of dimensionality more than analytical methods. This study investigates the impact of stochastic error in AMD models on OUP for low Earth orbit (LEO) satellites. The solution to the OUP problem is obtained by analytically solving the FPE using the Adomian decomposition (AD) method. The AD method is first applied to OUP in this study by approximating the time-varying PDF of the orbital state. The two-body motion model with non-conservative atmospheric drag is used to evaluate the AD solution. This solution shows a good agreement with the MCS result – a 0.1 m standard deviation of the orbital position (three-dimensional) from one-orbit propagation. This result also indicates the sensitivity of the OUP to the error associated with AMD models, which can be a reference for both space situational awareness and AMD modelling for LEO space objects.

Key Words: Orbital uncertainty propagation, Atmospheric mass density, Stochastic differential equation, Fokker-Planck equation, Adomian decomposition method

Nomenclature

$\boldsymbol{a_d}$	:	Atmospheric drag
$\mathfrak{B}, \mathfrak{B}_i$	:	Phase volume of the state $\boldsymbol{x}$ and its element x_i
B	:	Ballistic coefficient
C_i	:	Probability current of in the Fokker-Planck equation
$\boldsymbol{f}$	:	Deterministic forces
$\boldsymbol{g}$	:	Stochastic forces
$\boldsymbol{S}$	:	Diffusion coefficient vector
H	:	Scale height in the atmospheric mass density model
$\mathcal{L}_{FP}$	:	Fokker-Planck operator
$\mathcal{L}_t$	:	Partial differential operator with respect to time t
p	:	Transition probability density function or probability density function
$\boldsymbol{Q}, Q$	:	Time-invariant correlation matrix and correlation of Wiener process
$\boldsymbol{x}$	:	Orbital state vector
$\boldsymbol{r}, r$	:	Position in the Earth-centred inertial frame and its norm
$\boldsymbol{v}, v$	:	Inertial velocity in ECI and its norm
t	:	time
$\boldsymbol{v_r}, v_r$	:	Relative velocity in ECI and its norm
$\boldsymbol{W}, W$	:	m- and one-dimensional zero mean Wiener process
R_E	:	Earth radius
$\boldsymbol{\omega_E}$	:	Earth rotation vector
μ	:	Earth gravitation constant
ρ	:	Atmospheric mass density
Subscripts		
0	:	Initial
i, j	:	Generic indexes

1. Introduction

The collision of satellites between Iridium 33 and Kosmos-2251 on February 10, 2009 has called for more attention to space situational awareness of Earth-orbiting objects including active satellites and debris. The representation of orbital uncertainty propagation (OUP) plays a substantial role in space risk analysis. In addition, OUP is also critical for many aerospace engineering applications, such as re-entry analysis and orbit control of space objects.

Generally, the uncertainty can be categorised into three types: (1) epistemic uncertainty (systematic bias), (2) aleatory uncertainty (stochastic uncertainty) and (3) uncertainty due to human errors.[1)] In OUP, the first two types are resulting from an imperfect knowledge of orbital dynamics and randomness in the dynamical systems, respectively. Traditional OUP methods for deterministic (diffusionless) dynamical systems only deal with the aleatory uncertainties of the initial orbital state. Those OUP methods for the non-linear systems include Monte Carlo simulations (MCS), multi-Gaussian and non-Gaussian closure,[2,3)] polynomial chaos expansion,[2)] and state transition tensors.[4,5)]

Most of these methods, except for MCS, are developed for approximating the actual probability density function (PDF) with a few number of parameters, e.g., the first *N*th moments. Although the MCS can capture the revolution of PDF, it involves giant sampling of the state vector according to its probability distribution. This process needs extensive computation and thus to be time-consuming for long-term orbital propagation. In addition, other OUP methods such as Gaussian closure rely on the assumption of Gaussian distribution and only an approximate uncertainty (e.g., mean and covariance) is propagated forward in time with linear or higher order error propagation theory.[6] This approximation may lead to significant errors for long-term propagation of non-linear orbital dynamical systems.[7]

On the other hand, only a few studies have been carried out for those orbital dynamical systems perturbed by stochastic forces (diffusion).[7–9] Although the stochastic forces are very small, e.g., the stochastic forces from the error in atmospheric mass density (AMD) models, they may exert a large effect on the propagation of orbital uncertainty.[10] The evolution of a diffusion system can be described by an Itô stochastic differential equation (SDE) if the random error is a stationary Markov process, e.g., stationary Gaussian white noise (GWN).[11,12] Moreover, dynamical systems disturbed by other stationary processes with zero initial state and independent increments (e.g., the Poisson white noise and Lévy noise) can also be modelled with SDE.[13,14]

Currently, a powerful tool for the OUP problems of both deterministic and stochastic dynamical systems is the Fokker-Planck equation (FPE), which is a partial differential equation capturing the evolution of orbital uncertainty by propagating PDF or transition PDF (TPDF, or termed as conditional PDF).[15] Nevertheless, the FPE is very difficult to solve and its exact analytical solutions only exists for limited dynamical systems. Therefore, many studies have been carried out to numerically solve the FPE using methods such as the tensor decomposition, finite element approach, and path integral method.[14–16] However, the curse of dimensionality becomes even more serious for the numerical techniques. As an alternative, the Adomian decomposition (AD) method can provide an analytical solution to FPE.[17] It is a computationally effective methods, compared with the numerical methods, for linear or nonlinear, deterministic or stochastic operator equations such as ordinary differential equations (ODE), integral equations and partial differential equations.[18] The studies in Ref. 19, 20) show that the AD method can provide an approximate solution in an efficient way during a short period of time.

The OUP for a stochastic dynamical system still remains unsolved because of its computational burden and the curse of dimensionality. In this study, the AD method is applied to solving the FPE of orbital dynamics. The outline of the rest of the paper is as follows. Section **2.** introduces the FPE of stochastic dynamical systems and its properties and Section **3.** reviews the AD method and its application in solving FPE and some relevant conclusions are presented. Section **4.** elaborates the implement of using the AD moethod to solve the FPE and AD method in details, followed by a numeric example to evaluate the new method. Section **6.** presents the Conclusions.

2. Fokker-Planck Equation

The FPE, or forward Kolmogorov equation, depicts the evolution of the PDF of a stochastic dynamic system associated with an Itô process[5]

$$\mathrm{d}\boldsymbol{x} = \boldsymbol{f}(\boldsymbol{x},t)\,\mathrm{d}t + \boldsymbol{g}(\boldsymbol{x},t)\,\mathrm{d}\boldsymbol{W}(t), \tag{1}$$

where $\boldsymbol{x}(t) \in \mathbb{R}^n$ is a n-dimensional state vector (position-velocity); $\mathrm{d}\boldsymbol{x} = [\mathrm{d}x_i]^T \in \mathbb{R}^n$; $\boldsymbol{f}(\boldsymbol{x},t) : \mathbb{R}^n \times [0,\infty] \to \mathbb{R}^n$ denotes the deterministic terms of the dynamical systems; $\boldsymbol{g}(\boldsymbol{x},t) : \mathbb{R}^n \times [0,\infty] \to \mathbb{R}^{n\times m}$ denotes the stochastic terms (diffusion); $\boldsymbol{W}(t)_{t\in(0,T)} = [W_i(t)]^T$ $(i = 1,2,\ldots,m)$ is a m-dimensional zero mean Wiener process (the Brownian motion) with a correlation function

$$\mathbb{E}\left\{\mathrm{d}\boldsymbol{W}(t)\,\mathrm{d}\boldsymbol{W}^T(s)\right\} = \delta(t-s)\,\boldsymbol{Q}\mathrm{d}t, \tag{2}$$

where δ is the Dirac delta function; Q is the time-varying correlation matrix (or diffusion matrix) with a size of $n\times m$. The $\boldsymbol{f}$ and $\boldsymbol{g}$ are supposed to be continuous and bounded in $\mathbb{R}^n$, which can generally be satisfied in most of physical problems.

The evolution of the TPDF (or conditional PDF) is governed by the FPE[11,12]

$$\frac{\partial}{\partial t} p(\boldsymbol{x},t\,|\,\boldsymbol{x}_0,0) = \mathcal{L}_{FP}\left(p(\boldsymbol{x},t\,|\,\boldsymbol{x}_0,0)\right), \tag{3}$$

where

$$\begin{aligned}\mathcal{L}_{FP}(.) = &-\sum_{i=1}^{n}\frac{\partial}{\partial x_i}\left[\boldsymbol{f}(\boldsymbol{x},t)(.)\right]_i \\ &+\frac{1}{2}\sum_{i=1}^{n}\sum_{j=1}^{n}\frac{\partial^2}{\partial x_i \partial x_j}\left[\boldsymbol{S}(\boldsymbol{x},t)(.)\right]_{ij},\end{aligned} \tag{4}$$

$$\underset{n\times n}{\boldsymbol{S}}(x,t) = \boldsymbol{g}(\boldsymbol{x},t)\;Q(t)\;\boldsymbol{g}^T(\boldsymbol{x},t). \tag{5}$$

Here $\mathcal{L}_{FP}(.)$ is the FPE operator for n-dimensional variables, $\boldsymbol{f}(\boldsymbol{x},t)$ and $\boldsymbol{S}(\boldsymbol{x},t)$ are known as the drift coefficient vector and diffusion coefficient matrix (non-negative definite); $\boldsymbol{x}_0 \in \mathbb{R}^n$ is the initial state of $\boldsymbol{x}$ whose expectation and covariance are $\boldsymbol{\mu}$ and $\boldsymbol{\Sigma}$, respectively; subscript i represents the ith element of a vector and the index ij represents the (i,j) element of a matrix; $p(\boldsymbol{x},t\,|\boldsymbol{x}_0,0) : \mathbb{R}^n \times [0,\infty] \to [0,1]$ is the TPDF centred at $\boldsymbol{x}_0$ with the the normalisation condition

$$\int_{\mathfrak{B}} p(\boldsymbol{x},t\,|\,\boldsymbol{x}_0,0)\,\mathrm{d}^n\boldsymbol{x} = 1, \tag{6}$$

which ensures the solution of the FPE to be a valid TPDF, whose moments of arbitrary order are assumed to be existed and finite. In addition, the initial condition with respect to $\boldsymbol{x}_0$ will satisfy[15]

$$\lim_{t\to 0} p(\boldsymbol{x},t\,|\,\boldsymbol{x}_0,0) = \delta(\boldsymbol{x}-\boldsymbol{x}_0), \tag{7}$$

where $\mathfrak{B} = \mathfrak{B}_1 \times \cdots \times \mathfrak{B}_n$ $(\mathfrak{B}_i \in \mathbb{R})$ is the time-invariant phase volume of $\boldsymbol{x}$. The expression $\int_{\mathfrak{B}}(.)\,\mathrm{d}^n\boldsymbol{x}$ denotes $\int_{\mathfrak{B}_1}\cdots\int_{\mathfrak{B}_n}(.)\,\mathrm{d}x_1\cdots\mathrm{d}x_n$. Note that the phase volume can be either natural boundaries ($\pm\infty$) or a finite real space. The relationship between the PDF and TPDF of $\boldsymbol{x}$ for a Markov random process can be expressed by

$$p(\boldsymbol{x},t) = \int_{\mathfrak{B}} p(\boldsymbol{x},t\,|\,\boldsymbol{x}_0,0)\cdot p(\boldsymbol{x}_0,t)\,\mathrm{d}^n\boldsymbol{x}_0, \tag{8}$$

where $p(\boldsymbol{x}, t) : \mathbb{R}^n \times [0, \infty] \rightarrow [0, 1]$ is the PDF of $\boldsymbol{x}$ and $p(\boldsymbol{x}, t)|_{t=0} = p(\boldsymbol{x}_0, 0)$ is the initial PDF of $\boldsymbol{x}$ at the time of t. Taking the limits to both sides of Eq. (8) as t approaches to 0 yields Eq. (7).

Since the FPE is also applicable to PDF (proof refers to Appendix A):

$$\frac{\partial}{\partial t} p(\boldsymbol{x}, t) = \mathcal{L}_{FP}\left(p(\boldsymbol{x}, t)\right). \tag{9}$$

All the formulas above for the TPDF can be applied to PDF, except for its initial condition. Although, the FPE in the form of PDF is used in the following of this paper, similar equations for the TPDF can also be obtained.

The FPE in Eq.(3) is essentially a partial differential equation problem. Ref. 5) showed that the normalisation condition in Eq.(6) can be satisfied in any dynamical system without diffusion terms. However, this condition can be extensively applied to any dynamical system if following boundary conditions are satisfied at time t

$$\begin{aligned} \lim_{\boldsymbol{x}\to\sup(\mathfrak{B})} p(\boldsymbol{x}, t) &= \lim_{\boldsymbol{x}\to\inf(\mathfrak{B})} p(\boldsymbol{x}, t) = 0, \\ \lim_{\boldsymbol{x}\to\sup(\mathfrak{B})} \frac{\partial}{\partial \boldsymbol{x}} p(\boldsymbol{x}, t) &= \lim_{\boldsymbol{x}\to\inf(\mathfrak{B})} \frac{\partial}{\partial \boldsymbol{x}} p(\boldsymbol{x}, t) = \boldsymbol{0}_{n\times 1}, \end{aligned} \tag{10}$$

where sup and inf indicate the boundaries of the $\mathfrak{B}$. Refer to Appendix B for detailed proof.

Note that Eq. (10) is a sufficient but not the necessary condition for the normalisation condition. Usually, this pair of equations hold true for most of statistical distributions (e.g., the Gaussian normal distribution), otherwise $\int_{\mathfrak{B}} p(\boldsymbol{x}, t)\mathrm{d}^n\boldsymbol{x} > \infty$. In addition, the k-th moment of the initial PDF is assumed to be existed, i.e., $\int_{\mathfrak{B}} \boldsymbol{x}^k p(\boldsymbol{x}, t)\mathrm{d}^n\boldsymbol{x} < \infty$.

The following two properties can be derived from the definition of FPE in Eq. 3

(1) The FPE operator is a linear operator.

Considering two PDFs $\mathscr{A}$ and $\mathscr{C}$ from the space $\mathfrak{B} \times [0, +\infty]$ to $[0, 1]$:

$$\mathcal{L}_{FP}\left(a \cdot \mathscr{A} + c \cdot \mathscr{C}\right) = a\,\mathcal{L}_{FP}\left(\mathscr{A}\right) + c\,\mathcal{L}_{FP}\left(\mathscr{C}\right), \tag{11}$$

where a and c are real constants. This property can be used to speed up the computation of Adomian series in parallel (shown in Section **5.**).

(2) The expectations of the state for the SDE problem and its corresponding ODE problem are identical.

Applying expectations to both sides of Eq. (1) and using the boundary conditions given in Eq. (9) yields

$$\mathbb{E}(\boldsymbol{x}, t) = \int_0^t \int_{\mathfrak{B}} p(\boldsymbol{x}, \tau) \boldsymbol{f}(\boldsymbol{x}, \tau)\, \mathrm{d}^n\boldsymbol{x}\mathrm{d}\tau. \tag{12}$$

The corresponding deterministic dynamical system to the SDE system is given by the following:

$$\mathrm{d}\boldsymbol{x} = \boldsymbol{f}(\boldsymbol{x}, t)\, \mathrm{d}t, \tag{13}$$

which has the same expectation as that given by Eq. (12).

The results reveal that the stochastic forces in a SDE system do change the propagation of PDF but the expectation of the state will remain the same.

3. Application of AD method in FPE

3.1. Principle of AD method

Rewriting the FPE in Eq. (3) in the form of PDF[21] leads to

$$\mathcal{L}_t\left(p(\boldsymbol{x}, t)\right) = \mathcal{L}_{FP}\left(p(\boldsymbol{x}, t)\right), \tag{14}$$

where $\mathcal{L}_t(p) = \frac{\partial p}{\partial t}$, and p can be an arbitrary PDF. If the inverse operator of $\mathcal{L}_t(.)$ is existed, it can be given by the following definite integral with respect to τ from 0 to t

$$\mathcal{L}_t^{-1}(.) = \int_0^t (.)\mathrm{d}\tau, \tag{15}$$

Applying the operator to both sides of Eq. (14) yields

$$p(\boldsymbol{x}, t) = p(\boldsymbol{x}, 0) + \mathcal{L}_t^{-1}\left(\mathcal{L}_{FP}(p)\right). \tag{16}$$

$p(\boldsymbol{x}, t)$ can be expressed by a sum of components:

$$p(\boldsymbol{x}, t) = \sum_{i=0}^{\infty} p_i(\boldsymbol{x}, t), \tag{17}$$

where $p_i(\boldsymbol{x}, t)$ is determined by the following recursive equations:

$$\begin{cases} p_0(\boldsymbol{x}, t) = p(\boldsymbol{x}, 0) \\ p_{i+1}(\boldsymbol{x}, t) = \mathcal{L}_t^{-1}\left(\mathcal{L}_{FP}(p_i)\right)\ (i \geq 0) \end{cases} \tag{18}$$

We can find that $\int_{\mathfrak{B}} p(\boldsymbol{x}, t)\mathrm{d}^n\boldsymbol{x}$ is also an integral invariant if $p_0(\boldsymbol{x}, t)$ meet the condition in Eq. (10) (see Appendix C for more details), although $p_i(\boldsymbol{x}, t)(i \geq 1)$ is not a strict non-negative distribution function. Now the N order approximation of the solution is defined as $\phi_N(\boldsymbol{x}, t) = \sum_{i=0}^{N} p_i(\boldsymbol{x}, t)$.

3.2. Properties of the AD method

3.2.1. Convergence of the AD method

The convergence of the AD method has been proved using fixed point theorems under two given assumptions: (1) the solutions of a differential equation can be expressed as a series of functions which is assumed to be absolutely convergent and (2) the convergence radius of the Adomian polynomials is equal to infinity.[22–24] Refs. 25, 26) show that convergence of the AD method is not limited to these two assumptions and the fixed-point theorem. The convergence on AD method for non-contractive non-linear equation has been investigated in Ref. 27). Nevertheless, the speed of convergence is the largest limitation for the AD method, especially for the high order differential or high dimension problems.

Note that the AD method is essentially based on the Adomian series, which is an advantageous rearrangement of the Banach-space in computation similar to the Taylor expansion series.[18] The choice of decomposition in AD method is not unique.[18] It provides an advantageous characteristic to design the recursion schemes of AD method. For instance, convergence parameters are introduced into the AD method in order to achieve larger effective regions of convergence.[18,28] In this study, an improved recursive method of AD method is proposed with a convergence parameter, which is determined from the solutions to the corresponding ODE problem (see Section **4.**).

3.2.2. Moment of the PDF solution to FPE

The propagation of PDF using AD method can provide more information of interest than traditional way, e.g., propagation of expectation and covariance. Nevertheless, the expectation and covariance (or the first and second moments) are still used as two benchmarks in this study to evaluate the improved AD method. Substituting Eq. (17) into the kth moment of $\boldsymbol{x}$ at the epoch of t:

$$\begin{aligned}\mathbb{E}(\boldsymbol{X}^k, t) &= \int_{\mathfrak{B}} p(\boldsymbol{x}, t) \cdot \boldsymbol{x}^k \mathrm{d}^n \boldsymbol{x} \\ &= \sum_{i=0}^{\infty} \left(\int_{\mathfrak{B}} p_i(\boldsymbol{x}, t) \cdot \boldsymbol{x}^k \mathrm{d}^n \boldsymbol{x} \right) = \sum_{i=0}^{\infty} \mathbb{E}_i^k(t).\end{aligned} \tag{19}$$

where $\boldsymbol{X}$ indicates the random variables whose PDF is $p(\boldsymbol{x}, t)$; $\mathbb{E}_i^k(t)$ is the kth moment for the PDF $p_i(\boldsymbol{x}, t)$.

This means that the moment of $p(\boldsymbol{x}, t)$ is the sum of $\mathbb{E}_i^k(t)$ determined by $p(\boldsymbol{x}, t)$. Applying Eqs. (10) and (18) to the equation above, the first two moments for the PDF $p_m(\boldsymbol{x}, t)$ can be simplified as

$$\mathbb{E}_m^1(t) = \int_0^t \left(\int_{\mathfrak{B}} p_{m-1}\, \boldsymbol{f}(\boldsymbol{x}, \tau) \mathrm{d}^n \boldsymbol{x} \right) \mathrm{d}\tau, \tag{20}$$

$$\begin{aligned}\mathbb{E}_m^2(t) = \frac{1}{2} \int_0^t \Bigg[\int_{\mathfrak{B}} \Big(&\boldsymbol{S}(\boldsymbol{x}, \tau) + \boldsymbol{f}(\boldsymbol{x}, \tau) \cdot \boldsymbol{x}^T \\ &+ \boldsymbol{x} \cdot \boldsymbol{f}^T(\boldsymbol{x}, \tau) \Big)\, p_{m-1}\, \mathrm{d}^n \boldsymbol{x} \Bigg] \mathrm{d}\tau.\end{aligned} \tag{21}$$

The moments for higher orders can be derived but are excluded here for complexity. To be more general, for a given differentiable and continuous scalar function $h(\boldsymbol{x}, t)$, we have

$$\begin{aligned}&\int_{\mathfrak{B}} h(\boldsymbol{x}, t)\, p_m\, \mathrm{d}^n \boldsymbol{x} \\ &= \int_0^t \left[\int_{\mathfrak{B}} \left(-\sum_{i=1}^{n} f_i \frac{\partial h}{\partial x_i} + \frac{1}{2} \sum_{i=1}^{n} \sum_{j=1}^{n} S_{ij} \frac{\partial^2 h}{\partial x_i \partial x_j} \right) p_{m-1}\, \mathrm{d}^n \boldsymbol{x} \right] \mathrm{d}t,\end{aligned} \tag{22}$$

which is obtained assuming that the products of $h(\boldsymbol{x}, t)$ and p_m vanish on the boundary of $\mathfrak{B}$.

$$\begin{aligned}&\lim_{\boldsymbol{x} \to \sup(\mathfrak{B})} h(\boldsymbol{x}, t)\, p_m = \lim_{\boldsymbol{x} \to \inf(\mathfrak{B})} h(\boldsymbol{x}, t)\, p_m = 0, \\ &\lim_{\boldsymbol{x} \to \sup(\mathfrak{B})} h(\boldsymbol{x}, t) \frac{\partial p_m}{\partial \boldsymbol{x}} = \lim_{\boldsymbol{x} \to \inf(\mathfrak{B})} h(\boldsymbol{x}, t) \frac{\partial p_m}{\partial \boldsymbol{x}} = \boldsymbol{0}_{n \times 1}.\end{aligned} \tag{23}$$

4. OUP in static orbital dynamics

The orbital dynamics of LEO satellites with no diffusion term can be expressed by Eq. (13), in which $\boldsymbol{x}$ is in the Earth-centered inertial (ECI) Cartesian frame; $\boldsymbol{f}(\boldsymbol{x}, t) : \mathbb{R}^6 \times [0, +\infty] \to \mathbb{R}^6$ can include Earth gravitational force, N-body attraction, solar radiation pressure, and atmospheric drag, Earth albedo radiation pressure, Earth infrared radiation pressure, etc.[29] For simplicity, only two-body motion perturbed by atmospheric drag is considered in this study which can be formulated as

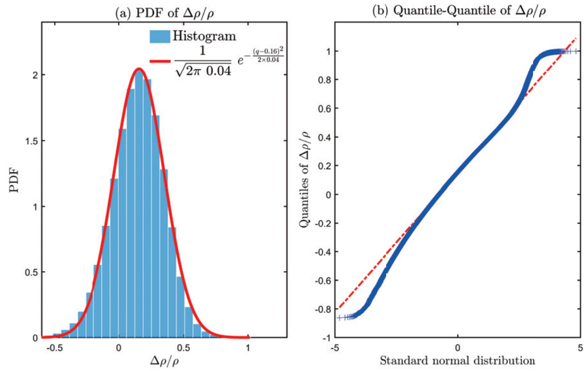

Fig. 1. Histogram of $q = \Delta\rho/\rho$ (a) and Quantile-Quantile plot between q and a standard Gaussian distribution (b); q is the ratio of error in DTM2012-model-derived AMD ($\Delta\rho$) to the model-derived AMD (ρ). The reference AMD values are derived from accelerometer measurements collected from the GRACE-A satellite in 2009.

$$d\boldsymbol{x} = \begin{bmatrix} \boldsymbol{v} \\ -\frac{\mu}{r^3}\boldsymbol{r} + \boldsymbol{a}_d \end{bmatrix} \mathrm{d}t, \quad \boldsymbol{x} = \begin{bmatrix} \boldsymbol{r}_{3\times1} \\ \boldsymbol{v}_{3\times1} \end{bmatrix}, \tag{24}$$

$$\boldsymbol{a}_d(\boldsymbol{x}) = -\frac{1}{2} \rho\, B\, |\boldsymbol{v}_r|\, \boldsymbol{v}_r, \tag{25}$$

$$\boldsymbol{v}_r(\boldsymbol{x}) = -\boldsymbol{v} + \boldsymbol{\omega}_E \times \boldsymbol{r}, \tag{26}$$

$$\rho(\boldsymbol{x}) = \rho_0\, e^{-\frac{|\boldsymbol{r}| - R_E}{H}}, \tag{27}$$

where $\boldsymbol{a}_d$ is the atmospheric drag; $\boldsymbol{v}_r$ is the satellite velocity relative to the atmosphere; B is the ballistic coefficient; $\boldsymbol{\omega}_E$ is the Earth's angular velocity vector; $|\,.\,|$ is the Euclidean distance. The AMD ρ in Eq. (27) is assumed to follow a time-invariant exponential model with reference AMD ρ_0.

If $\tilde{\boldsymbol{a}}_d$ is the 'true' acceleration due to the atmospheric drag, the noise $\Delta\rho$ in the AMD can be expressed by a ratio q

$$\begin{aligned}\tilde{\boldsymbol{a}}_d &= -\frac{1}{2} \tilde{\rho}\, B\, |\boldsymbol{v}_r|\, \boldsymbol{v}_r = -\frac{1}{2} (\rho + \Delta\rho)\, B\, |\boldsymbol{v}_r|\, \boldsymbol{v}_r \\ &= -\frac{1}{2} \rho\, B\, |\boldsymbol{v}_r|\, \boldsymbol{v}_r \left(1 + \frac{\Delta\rho}{\rho} \right) = -\frac{1}{2} \rho\, B\, |\boldsymbol{v}_r|\, \boldsymbol{v}_r\, (1 + q)\,.\end{aligned} \tag{28}$$

Figure 1 gives the histogram and the fitting PDF curve (in red) of $\Delta\rho/\rho$ determined from the state-of-the-art AMD model – DTM2012[30] and accelerometer measurements from the GRACE-A satellite in 2009. These data are provided by Ref. 31). Note that those ratio values out of $\mu \pm 5\sigma$ are excluded as outliers. The outlier deletion rate is around 0.012%. The red curve in Fig. 1(a) indicates a standard Gaussian distribution. Figure 1(b) gives the Quantile-Quantile plot of the quantiles of q versus theoretical quantiles from a normal Gaussian distribution.

This results show that the relative error $\Delta\rho/\rho$ approximately follows a Gaussian distribution, i.e., $\Delta\rho/\rho \sim \mathcal{N}(0.16, 0.04)$. If the bias of 0.16 is neglected, the aforementioned Itô process (see Section **2.**) can be used to depict the orbital dynamics of the two-body problem.

Consequently, the continuous-time system subjected to the stochastic error ($\Delta\rho/\rho$) in AMD can be expressed as

$$d\boldsymbol{x} = \begin{bmatrix} \boldsymbol{v} \\ -\frac{\mu}{r^3}\boldsymbol{r} + \boldsymbol{a}_d \end{bmatrix} \mathrm{d}t + \begin{bmatrix} \boldsymbol{0}_{3\times1} \\ \boldsymbol{a}_d \end{bmatrix} dW(t), \tag{29}$$

where $W(t)$ is an one-dimensional zero-mean standard Wiener process and its correlation factor Q is reduced to be a constant scalar.

In this dynamical system, the epistemic uncertainty (systematic error) in AMD is neglected for simplicity and, consequently, the drift term from the uncertainty of AMD is not shown in Eq. (29). Nevertheless, its drift effect can be easily modelled by adding a term into the deterministic forces. It is worth noting that $\boldsymbol{v}_r$ in Eq. (26) is not the wind velocity of the atmosphere, since its impact on the OP of LEO satellites is found not significant. The maximum difference between in the 3D-orbit of the GRACE-A ($\sim$ 500 km) propagated with and without wind models during one-day propagation in solar minimum is less than 3m (not shown in this study). The horizontal wind model (HWM07)[32] is used in this evaluation.

As a result, Eq. (9) can be rewritten as

$$\frac{\partial p(\boldsymbol{x},t)}{\partial t} = -\sum_{i=1}^{6}\frac{\partial}{\partial x_i}\left[f_i \cdot p\right] + \frac{1}{2}\sum_{i=4}^{6}\sum_{j=4}^{6}\frac{\partial^2}{\partial x_i \partial x_j}\left[S_{ij}\cdot p\right]. \tag{30}$$

Substituting Eq. (29) into the above equation yields

$$\begin{aligned}\mathcal{L}_{FP}(p) &= 2\rho\, B\,|\boldsymbol{v}_r|\, p - \boldsymbol{f}^T \cdot \frac{\partial p}{\partial \boldsymbol{x}} \\ &+ \frac{1}{8}B^2\rho^2\, Q\,|\boldsymbol{v}_r|^2\left(12\,\boldsymbol{v}_r{}^T\cdot\frac{\partial p}{\partial \boldsymbol{v}}\right. \\ &\left. + \operatorname{vec}\left(\boldsymbol{v}_r{}^T\boldsymbol{v}_r\right)^T \cdot \operatorname{vec}\left(\frac{\partial^2 p}{\partial \boldsymbol{v}\,\partial \boldsymbol{v}^T}\right) + 30p\right),\end{aligned} \tag{31}$$

where 'vec' is the reshaping process that stacks one column of a matrix underneath the previous one.

Since the orbital dynamical system defined in Eq. (29) is static, the approximate solution to the FPE derived from the AD method can be simplified as

$$\phi_N(\boldsymbol{x},t) = \sum_{i=0}^{N}\frac{t^i}{i!}\mathcal{L}_{LP}^{(i)}(p_0). \tag{32}$$

Taking the expectation of both sides of Eq. (29), this SDE dynamical system will be reduced to the ODE dynamical system expressed by Eq. (24) since the drift effect of the stochastic force in Eq. (29) is not considered. Therefore, the expectation of the states in the SDE at a specific time is identical to that in the corresponding ODE problem at the same epoch. This property has been used to validate the results of the AD method in this study.

To improve the convergence of the Adomian series, a convergence parameter $q(\boldsymbol{x},t) = \sum_{i=0}^{\infty} q_i(\boldsymbol{x},t)$ is substituted into Eq. (18)

$$\begin{cases} u_0 = q(\boldsymbol{x},t) \\ u_{i+1} = \mathcal{L}_t^{-1}\left(\mathcal{L}_{FP}(p_i)\right) - \mathcal{L}_t^{-1}\left(\mathcal{L}_D(q_i)\right)\ (i \geq 0), \end{cases} \tag{33}$$

where

$$\mathcal{L}_D(.) = -\sum_{i=1}^{n}\frac{\partial}{\partial x_i} f_i(\boldsymbol{x},t)(.), \tag{34}$$

$$\begin{cases} q_0 = p(\boldsymbol{x},0) \\ q_{i+1} = \mathcal{L}_t^{-1}(\mathcal{L}_D(q_i))\ (i \geq 0). \end{cases} \tag{35}$$

One may notice that $q(\boldsymbol{x},t)$ is in fact the AD-derived approximate solution to the corresponding ODE problem defined in Eq. (24). Since the stochastic forces will not modify the expectation of the orbital state (Section **3.**), the expectation of u_i ($i \geq 1$) is zero, i.e., the first moment of $u(\boldsymbol{x},t)$ can be estimated without error. Moreover, its covariance matrix can be expressed by

$$\mathbb{D}(\boldsymbol{X},t) = \sum_{i=3}^{\infty}\left(\int_{\mathfrak{B}} u_i(\boldsymbol{x},t)\,\boldsymbol{x}\boldsymbol{x}^T \mathrm{d}^n\boldsymbol{x}\right). \tag{36}$$

where the contributions of u_1 and u_2 are zero due to $p_1 = q_1$ and $p_2 = q_2$.

Since the total number of the terms in u_i will be exponentially increased, the parallel computation is adopted in determination of the u_i according to the linearity of FPE operator given in Eq. (11).

5. Results and discussions

In this section, results of OUP for an example of LEO satellites are presented and it is assumed that the initial state of the LEO satellite is accurately known

$$\boldsymbol{x}_0 = \begin{bmatrix} 1571946.9778\,m \\ -542449.7712\,m \\ -6634410.9086\,m \\ 7153.3854\,m/s \\ -1891.6220\,m/s \\ 1854.9557\,m/s \end{bmatrix}.$$

This example corresponds to a initial orbit with an altitude of 470 km and a period of 93.5 min. Therefore, the initial PDF of the orbital state is a Dirac delta function $p(\boldsymbol{x},0) = \delta(\boldsymbol{x}-\boldsymbol{x}_0)$. The corresponding ODE problem to this SDE problem is deterministic and uncertainty-free and its solution can be determined accurately (termed as $\boldsymbol{x}_s(t)$). As a result, $q(\boldsymbol{x},t)$ in Eq. 33 becomes $\delta(\boldsymbol{x} - \boldsymbol{x}_s(t))$. This example of two-body motion is selected in this study for two reasons: (1) the uncertainty of the initial orbital state can be excluded in this study and (2) determination of the expectations and covariances of the orbital state can be simplified using the properties of the Dirac Delta function.[33]

In this example, the atmospheric drag is only perturbation force considered. The settings of the other parameters in Eq. (29) are $B = 0.0023$, $\rho_0 = 9\times10^{-13}\,kg/m^3$, $H = 65\,km$. The values of ρ_0 and H are estimated from the DTM2012-derived AMD using the least squares method. The time-invariant correlation of the one-dimensional Wiener process in Eq. (29) is assigned to one, i.e., $Q = 1$, indicating that the relative error $\Delta\rho/\rho$ falls within the interval $[-100\%, 100\%]$ for the probability of 0.68. Note that the noise in ρ is assumed to be bias-free. In this study, the Mathematica software is applied to running the MCS using the stochastic Runge-Kutta scheme. Of the MCS with the same initial orbital state, 5000 samples are propagated forward for one orbital period. The result of MCS is a benchmark for evaluating the AD method.

Figures 2 and 3 illustrate the expectation and standard deviation (σ) of the orbital position in one orbital period propagation. It can be seen that the trajectory of the satellite shows a clear periodic pattern resulting from the two-body motion.

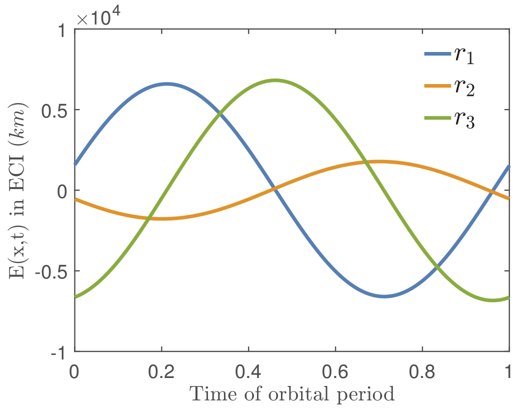

Fig. 2. Expectation of the three components of orbital position in ECI frame for one-orbital-period (∼ 93.5 *min*) propagation from MCS.

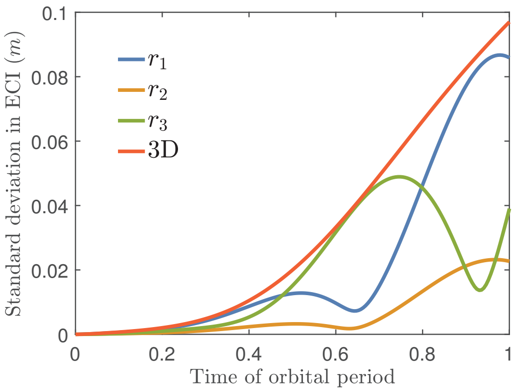

Fig. 3. Standard deviation of the orbital position (3D) and its three components (r_i) in ECI frame for one-orbital-period propagation from MCS.

More importantly, the impact of the random error in ρ is limited (σ of position) for one orbital period propagation. Whilst the AD method with order of five gives consistent OUP results as shown in Fig. (4). Only presented are standard deviation values, obtained from Eqs. (22) and (36), since the expectations are error-free.

Although the above results are from one-orbital-period only, the AD method may be applied to long-term propagation if its dominant limitation of convergence can be further improved. In addition, the computational burden involved in multi-dimensional integrals and differentials in the AD method is another limiting factor. A semi-analytical method based on the AD method is a better approach which represents PDF by specific functions, e.g., Fourier series[16] or Gaussian mixture.[7] For a short-term orbit propagation, however, the AD method shows a fast convergence as presented in this study. This results imply the applicability of the method to non-linear filtering problems[34]).

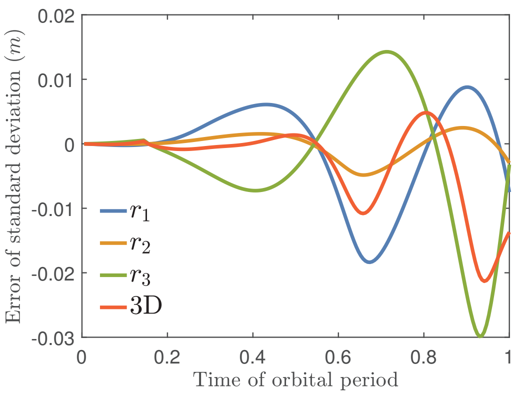

Fig. 4. Difference of the standard deviation of the orbital position (3D) and its three components (r_i) in ECI frame between MCS and AD method for one-orbital-period propagation.

6. Conclusions

OUP is of great importance in many aerospace engineering applications such as space situational awareness and orbit control. However, The OUP problem is not perfectly solved, especially for orbital dynamical systems perturbed by stochastic forces. This study presents an analytical approach based on the AD method for solving the FPE which depicts the evolution of PDF of an orbital dynamical system. A sufficient condition is identified for integral invariance of the PDF of orbital state for diffusion orbital dynamical systems. Also proved is that the AD method can keep the property of integral invariance to its solutions. In addition, it is found that stochastic forces will not change the expectation of the orbital states in stochastic dynamical systems.

The result of the AD method show its good agreement with that of MCS. However, both speed and region of convergence are the two limiting factors for the AD-based approach. To address these limitations, a convergence parameter and parallel computation can be adopted based on the linearity of the FPE operator. The standard deviation of orbital position resulting from the diffusion for one orbital period is less than 0.1 m. In future studies, the improved AD method will be applied to the OUP problem with uncertainty of the initial orbital states.

Acknowledgments

The authors would like to acknowledge the support of the Cooperative Research Centre for Space Environment Management (SERC Limited) through the Australian Government's Cooperative Research Centre Programme. Dr. Jérôme Daquin at RMIT University is appreciated for his helpful comments and suggestions.

A The FPE for transition PDF and PDF

Taking derivative of Eq. (8) with respect to time t

$$\begin{aligned}\frac{\partial p(\boldsymbol{x},t)}{\partial t} &= \frac{\partial}{\partial t}\int_{\mathfrak{B}} p(\boldsymbol{x},t\,|\,\boldsymbol{y},0)\cdot p(\boldsymbol{y},0)\,\mathrm{d}^n\boldsymbol{y} \\ &= \int_{\mathfrak{B}} \frac{\partial p(\boldsymbol{x},t\,|\,\boldsymbol{y},0)}{\partial t} p(\boldsymbol{y},0)\,\mathrm{d}^n\boldsymbol{y}.\end{aligned} \tag{A.1}$$

Upon substitution of the Eqs. (3)−(5) into the above equation, the following equation is obtained

$$\frac{\partial p(\boldsymbol{x},t)}{\partial t} = \int_{\mathfrak{B}} \mathcal{L}_{FP}\left(p(\boldsymbol{x},t\,\middle|\,\boldsymbol{y},0)\right)\cdot p(\boldsymbol{y},0)\,\mathrm{d}^n\boldsymbol{y}. \tag{A.2}$$

Since the derivative in the FPE operator is only with respect to $\boldsymbol{x}$, we thus have the following equation

$$\begin{aligned}\frac{\partial p(\boldsymbol{x},t)}{\partial t} &= \mathcal{L}_{FP}\left(\int_{\mathfrak{B}} p(\boldsymbol{x},t\,|\,\boldsymbol{y},0)\,p(\boldsymbol{y},0)\,\mathrm{d}^n\boldsymbol{y}\right) \\ &= \mathcal{L}_{FP}\left(p(\boldsymbol{x},t)\right).\end{aligned} \tag{A.3}$$

The proof shows that FPE is also applicable to PDF.

B Integral invariant of $\int_{\mathfrak{B}} p(\boldsymbol{x},t)d^n\boldsymbol{x}$

Define the probability current $C_i(\boldsymbol{x},t) : \mathbb{R}^n \times [0, +\infty] \to \mathbb{R}$ to be

$$\begin{aligned}C_i(\boldsymbol{x},t) &= -\mathcal{L}_{FP}\left(p(\boldsymbol{x},t)\right) \\ &= p(\boldsymbol{x},t)f_i(\boldsymbol{x},t) - \frac{1}{2}\sum_{j=1}^{n}\frac{\partial}{\partial x_j}p(\boldsymbol{x},t)\,D_{ij}.\end{aligned} \tag{B.1}$$

Then the FPE can be expressed as

$$\frac{\partial p(\boldsymbol{x},t)}{\partial t} + \sum_{i=1}^{n}\frac{\partial}{\partial t}C_i(\boldsymbol{x},t) = 0. \tag{B.2}$$

If the $C_i(\boldsymbol{x},t)\,(i = 1, 2, \ldots n)$ vanish at the boundaries of phase space $\mathfrak{B}$ (i.e., $x_i = sup(\mathfrak{B}_i)$ or $x_i = inf(\mathfrak{B}_i)$), then total probability $\int_{\mathfrak{B}} p(\boldsymbol{x},t)\,\mathrm{d}^n\boldsymbol{x}$ will be constant.[12] Here $\mathfrak{B}$ can be natural boundaries ($\pm\infty$) or a finite real space.

Keep in mind that $\boldsymbol{x}$ in the total probability $p(\boldsymbol{x},t)$ is not a function of time t. Hence, the derivative of total probability of PDF $p(\boldsymbol{x},t)$ with respect to time will be

$$\begin{aligned}\frac{\mathrm{d}}{\mathrm{d}t}\left(\int_{\mathfrak{B}} p(\boldsymbol{x},t)\,\mathrm{d}^n\boldsymbol{x}\right) &= \int_{\mathfrak{B}}\frac{\partial\, p(\boldsymbol{x},t)}{\partial t}\,\mathrm{d}^n\boldsymbol{x} \\ &= \int_{\mathfrak{B}} -\sum_{i=1}^{n}\frac{\partial}{\partial x_i}C_i(\boldsymbol{x},t)\,\mathrm{d}^n\boldsymbol{x} \\ &= -\sum_{i=1}^{n}\int_{\mathfrak{B}}\frac{\partial}{\partial x_i}C_i(\boldsymbol{x},t)\,\mathrm{d}^n\boldsymbol{x}.\end{aligned} \tag{B.3}$$

Considering the boundary condition of $C_i(\boldsymbol{x},t)$ presented as above, each term in the summation on the right side of Eq. (B.3) can be rewritten as

$$\int_{\mathfrak{B}}\frac{\partial}{\partial x_i}C_i(\boldsymbol{x},t)\,\mathrm{d}^n\boldsymbol{x} = \int_{\mathfrak{B}/\mathfrak{B}_i} C_i(\boldsymbol{x},t)\Big|_{x_i=inf(\mathfrak{B}_i)}^{x_i=sup(\mathfrak{B}_i)}\,\mathrm{d}^n\boldsymbol{x}/dx_i. \tag{B.4}$$

This result shows that if PDF is normalised to 1 at any time (e.g., at the initial time $t = 0$), or the normalisation condition of PDF will always hold. Specifically, the boundary condition of $C_i(\boldsymbol{x},t)$ can be reduced to

$$\begin{aligned}\lim_{x_i\to\sup(\mathfrak{B}_i)} p(\boldsymbol{x},t) &= \lim_{x_i\to\inf(\mathfrak{B}_i)} p(\boldsymbol{x},t) = 0, \\ \lim_{x_i\to\sup(\mathfrak{B}_i)}\frac{\partial}{\partial x_j}p(\boldsymbol{x},t) &= \lim_{x_i\to\inf(\mathfrak{B}_i)}\frac{\partial}{\partial x_j}p(\boldsymbol{x},t) = 0.\end{aligned} \tag{B.5}$$

These two equations are detailed format of Eq. (10). As readers may have noticed that these boundary conditions will be satisfied if any x_i approaches to its boundary.

C Integral invariant of $p_{i+1}(\boldsymbol{x},t)$ $(i \geqslant 0)$

By substituting the Eq. (18) into the integral of p_{n+1} with respect to $\boldsymbol{x}$ over $\mathfrak{B}$ domain, we have

$$\begin{aligned}&\int_{\mathfrak{B}} p_{n+1}(\boldsymbol{x},t)\,\mathrm{d}^n\boldsymbol{x} = \int_{\mathfrak{B}}\mathcal{L}_t^{-1}\left(\mathcal{L}_{FP}(p_n)\right)\,\mathrm{d}^n\boldsymbol{x} \\ &= \int_{\mathfrak{B}}\int_0^t\left\{-\sum_{i=1}^{n}\frac{\partial}{\partial x_i}\left[p_n(\boldsymbol{x},\tau)\,f_i(\boldsymbol{x},\tau)\right]\right. \\ &\quad\left.+\frac{1}{2}\sum_{i=1}^{n}\sum_{j=1}^{n}\frac{\partial^2}{\partial x_i\partial x_j}\left[p_n(\boldsymbol{x},\tau)\,S_{ij}(\boldsymbol{x},\tau)\right]\right\}\mathrm{d}t\,\mathrm{d}^n\boldsymbol{x} \\ &= \int_0^t\int_{\mathfrak{B}}\left\{-\sum_{i=1}^{n}\frac{\partial}{\partial x_i}\left[p_n(\boldsymbol{x},\tau)\,f_i(\boldsymbol{x},\tau)\right]\right. \\ &\quad\left.+\frac{1}{2}\sum_{i=1}^{n}\sum_{j=1}^{n}\frac{\partial^2}{\partial x_i\partial x_j}\left[p_n(\boldsymbol{x},\tau)\,S_{ij}(\boldsymbol{x},\tau)\right]\right\}\mathrm{d}^n\boldsymbol{x}\,\mathrm{d}t \\ &= \int_0^t\int_{\mathfrak{B}} -\frac{\partial}{\partial x_i}C_i(\boldsymbol{x},\tau)\mathrm{d}^n\boldsymbol{x}\,\mathrm{d}t.\end{aligned} \tag{C.1}$$

Based on the conclusions given in Appendix B, the term on the right side of Eq. (C.1) will be zero if $C_i(\boldsymbol{x},t)\Big|_{x_i=inf(\mathfrak{B}_i)}^{x_i=sup(\mathfrak{B}_i)} = 0$ or, specifically, if Eq. (B.5) is satisfied. It means that the approximate solution $\phi_N(\boldsymbol{x},t) = \sum_{i=0}^{N} p_i(\boldsymbol{x},t)$ to the FPE will always fulfil the normalisation condition if the condition for the initial PDF p_0 is satisfied. Similarly, the integral invariance of TPDF can be repeatedly derived from Eq. (8) and Appendix A. The proof will be skipped here owing to space constraints.

References

1) M. Razi, P. J. Attar, and P. Vedula. Adaptive numerical solutions of fokker-planck equations in computational uncertainty quantification. In *52nd AIAA/ASME/ASCE/AHS/ASC Structures, Structural Dynamics and Materials Conference 19th AIAA/ASME/AHS Adaptive Structures Conference 13t*, page 1976, 2011.
2) R. Madankan, P. Singla, T. Singh, and P. D. Scott. Polynomial-chaos-based bayesian approach for state and parameter estimations. *Journal of Guidance Control and Dynamics*, 36(4):1058–1074, 2013.
3) G. K. Er. Multi-gaussian closure method for randomly excited non-linear systems. *International Journal of Non-Linear Mechanics*, 33(2):201–214, 1998.
4) M. Majji, J. L. Junkins, and J. Turner. A high order method for estimation of dynamic systems. *Journal of the Astronautical Sciences*, 56(3):401–440, 2008.
5) R. S. Park and D. J. Scheeres. Nonlinear mapping of gaussian statistics: Theory and applications to spacecraft trajectory design. *Journal of Guidance Control and Dynamics*, 29(6):1367–1375, 2006.
6) B. Schutz, B. Tapley, and G. H. Born. *Statistical orbit determination*. Elsevier Academic Press, London, 2004.
7) D. Giza, P. Singla, and M. Jah. An approach for nonlinear uncertainty propagation: Application to orbital mechanics. In *AIAA Guidance, Navigation, and Control Conference, Chicago IL*, page 6082, 2009.
8) N. J. Kasdin. Runge-kutta algorithm for the numerical-integration of stochastic differential-equations. *Journal of Guidance Control and Dynamics*, 18(1):114–120, 1995.
9) Y. F. Sun and M. Kumar. Uncertainty propagation in orbital mechanics via tensor decomposition. *Celestial Mechanics and Dynamical Astronomy*, 124(3):269–294, 2016.
10) D. J. Scheeres, D. Han, and Y. Hou. Influence of unstable manifolds on orbit uncertainty. *Journal of Guidance Control and Dynamics*, 24(3):573–585, 2001.

11) P. E. Kloeden and E. Platen. *Numerical Solution of Stochastic Differential Equations*. Stochastic Modelling and Applied Probability. Springer, Berlin Heidelberg, 1992.
12) H. Risken. *The Fokker-Planck equation : methods of solution and applications*. Fokker-Planck Equation. Springer Verlag, Berlin, 2nd edition, 1996.
13) S. I. Denisov, W. Horsthemke, and P. Hanggi. Generalized fokker-planck equation: Derivation and exact solutions. *European Physical Journal B*, 68(4):567–575, 2009.
14) X. Sun and J. Q. Duan. Fokker-planck equations for nonlinear dynamical systems driven by non-gaussian levy processes. *Journal of Mathematical Physics*, 53(7):072701, 2012.
15) S. Narayanan and P. Kumar. Numerical solutions of fokker-planck equation of nonlinear systems subjected to random and harmonic excitations. *Probabilistic Engineering Mechanics*, 27(1):35–46, 2012.
16) M. Kumar, S. Chakravorty, P. Singla, and J. L. Junkins. The partition of unity finite element approach with hp-refinement for the stationary fokker-planck equation. *Journal of Sound and Vibration*, 327(1-2):144–162, 2009.
17) G. Adomian and R. Rach. Inversion of nonlinear stochastic operators. *Journal of Mathematical Analysis and Applications*, 91(1):39–46, 1983.
18) J. S. Duan, R. Rach, D. Baleanu, and A. M. Wazwaz. A review of the adomian decomposition method and its applications to fractional differential equations. *Communications in Fractional Calculus*, 3(2):73–99, 2012.
19) M. M. Saleh and I. L. El-Kalla. On the generality and convergence of adomian's method for solving partial differential equations. *International Journal of Differential Equations and Applications*, 7(1), 2011.
20) E. Babolian and J. Biazar. On the order of convergence of adomian method. *Applied Mathematics and Computation*, 130(2-3):383–387, 2002.
21) M. Tatari, M. Dehghan, and M. Razzaghi. Application of the adomian decomposition method for the fokker-planck equation. *Mathematical and Computer Modelling*, 45(5-6):639–650, 2007.
22) Y. Cherruault. Convergence of adomian's method. *Kybernetes*, 18(2):31–38, 1989.
23) L. Gabet. The theoretical foundation of the adomian method. *Computers & Mathematics with Applications*, 27(12):41–52, 1994.
24) M. M. Hosseini and H. Nasabzadeh. On the convergence of adomian decomposition method. *Applied Mathematics and Computation*, 182(1):536–543, 2006.
25) Y. Cherruault and G. Adomian. Decomposition methods: a new proof of convergence. *Mathematical and Computer Modelling*, 18(12):103–106, 1993.
26) R. C. Rach. A new definition of the adomian polynomials. *Kybernetes*, 37(7):910–955, 2008.
27) S. Ghosh, A. Roy, and D. Roy. An adaptation of adomian decomposition for numeric–analytic integration of strongly nonlinear and chaotic oscillators. *Computer Methods in Applied Mechanics and Engineering*, 196(4):1133–1153, 2007.
28) L. Lu and J. S. Duan. How to select the value of the convergence parameter in the adomian decomposition method. *Cmes-Computer Modeling in Engineering and Sciences*, 97(1):35–52, 2014.
29) M. Oliver and G. Eberhard. *Satellite orbits: models, methods and applications*. Springer Science and Business Media, 2012.
30) S. Bruinsma. Dtm2012 evaluation report. Report, Centre National d'Etudes Spatiales (CNES), 2012.
31) E. K. Sutton, R. S. Nerem, and J. M. Forbes. Density and winds in the thermosphere deduced from accelerometer data. *Journal of Spacecraft and Rockets*, 44(6):1210–1219, 2007.
32) D. P. Drob, J. T. Emmert, G. Crowley, J. M. Picone, G. G. Shepherd, W. Skinner, P. Hays, R. J. Niciejewski, M. Larsen, C. Y. She, J. W. Meriwether, G. Hernandez, M. J. Jarvis, D. P. Sipler, C. A. Tepley, M. S. O'Brien, J. R. Bowman, Q. Wu, Y. Murayama, S. Kawamura, I. M. Reid, and R. A. Vincent. An empirical model of the earth's horizontal wind fields: Hwm07. *Journal of Geophysical Research-Space Physics*, 113(A12), 2008.
33) E. W. Weisstein. Delta function, 2017.
34) M. Kumar and S. Chakravorty. Nonlinear filter based on the fokker-planck equation. *Journal of Guidance Control and Dynamics*, 35(1):68–79, 2012.